JOURNAL OF MATERIALS SCIENCE 18 (1983) 3363–3376

The variation of γ' particle size and volume fraction in Nimonic PE16 aged at 700°C

P. K. MADDEN, V. M. CALLEN
Central Electricity Generating Board, Berkeley Nuclear Laboratories, Berkeley, Gloucestershire, UK

A transmission electron microscopy technique is presented which enables γ' particle sizes and volume fractions to be determined quickly and reliably. Samples of solution-treated PE16 aged at 700° C for up to 10 000 h are investigated. The results obtained show that γ' precipitation is complete after 16 h ageing, the maximum volume fraction being ~ 9%. Thereafter the mean particle size ($\bar{d}$) and particle number density (ρ) vary with age time (t) in accordance with the following empirical relationships:

$$\bar{d} \propto t^{0.28}; \quad \rho \propto t^{-0.86}.$$

The errors incurred are discussed.

1. Introduction

The nickel-based superalloy Nimonic PE16 is strengthened by particles of the γ' ($Ni_3(Ti, Al)$) phase. Its precise strength is determined by the γ' particle size and volume fraction, which in turn, depend on the initial heat treatment of the alloy and its subsequent ageing during service [1].

The variation of particle size with age time in solution-treated PE16 has been investigated extensively, e.g. [1–3]. The data obtained are in fair agreement. There is however some disagreement regarding the quantity of γ' precipitation. For example Martens and Nembach [4] observe a volume fraction ~ 10% in PE16 aged at 750° C while Gelles [5] observes a maximum of only ~ 6%. This difference may reflect differences in initial heat treatments: (1250° C/4 h + 700° C/2 h) and (1040° C/4 h + 900° C/1 h), respectively.

A transmission electron microscopy (TEM) technique is presented which enables γ' particle sizes and volume fractions to be determined quickly and reliably. Samples of solution-treated PE16 aged at 700° C, for up to 10 000 h, are investigated.

Recently the small angle neutron scattering (SANS) technique has been used to obtain γ' particle size and volume fraction data [6]. The results obtained in a collaborative programme using the independent TEM and SANS techniques, will be presented elsewhere [7].

2. Experimental details

The chemical compositions of the alloys investigated are given in Table I. Samples of alloy I were taken from untested areas of strip tensile specimens stamped out of 0.38 mm thick 30% cold-worked strip, solution-treated in vacuo at 1040° C for 0.5 h and aged in vacuo at 700° C for up to 10 000 h prior to cooling in air [2]. Samples of alloy II were taken from a 10 mm diameter bar, solution treated at 1020–1060° C for 0.25 h and aged at 680–720° C for 2.5 h.

3 mm discs were punched out of the alloys and ground down to ~ 120 μm thickness on silicon carbide grit papers. They were electropolished to perforation in a Struers Tenupol unit using either, a 10% perchloric acid/90% methanol solution cooled to − 60° C, or, a 10% perchloric acid/90% 2-butoxyethonol solution at room temperature. One disc was electropolished in a unithin jet polishing machine using Lenoirs solution (78 g chromic oxide, 67 ml concentrated sulphuric acid, 310 ml phosphoric acid and 120 ml water) at room temperature.

The discs were examined in a Philips EM400T scanning transmission electron microscope (STEM)

0022–2461/83 $03.00 + .12

TABLE I Chemical compositions of the Nimonic PE16 alloys investigated

	Composition (wt %)												
	C	Si	Mn	S	Cr	Mo	Ni	Al	B	Co	Ti	Zr	Fe
Alloy I	0.047	0.22	0.06	0.003	16.6	3.22	43.6	1.19	0.002	0.27	1.20	0.035	Balance
Alloy II	0.05	0.26	0.03	0.006	16.66	3.21	43.6	1.13	0.003	0.05	1.15	0.02	Balance

using the transmission mode for particle size, number density and volume fraction determinations and the scanning mode for differential matrix/particle electropolishing effects. In every case an accelerating potential of 100 kV was used.

The discs were always positioned for eucentricity in the microscope. After each investigation an Agar S104 2160 lines mm^{-1} calibration grid was imaged under the same conditions.

3. Imaging and analysis

3.1. Imaging γ' particles

γ' particles were imaged in dark field superlattice reflections, High index reflections were used to reduce extraneous contrast from matrix reflections. Unbuckled areas of foil were selected with average thicknesses approximately equal to the diameter of the largest particle present. This ensured optimum image resolution and minimum particle overlap.

The specimen electropolished in Lenoirs solution was also imaged by phase contrast in bright field.

3.2. Foil thickness determination

Normally the foil thickness profile of a sample is determined by counting extinction contours imaged under 2-beam bright field conditions [8]. The measured extinction distances of the 1 1 1, 2 0 0 and 2 2 0 reflections in PE16 are 28, 32 and 44 nm, respectively [9]. Typically the average foil thickness is 10 to 100 nm and the method is rather insensitive. The weak beam technique is used here [10]. The sample is imaged in a centred dark field reflection **g**. It is tilted to excite a higher order reflection $n\mathbf{g}$. The extinction distance ξ_g reduces to an effective value ξ_g^{eff} [8].

$$\xi_g^{eff} = \xi_g/(1 + s^2\xi_g^2)^{1/2} \quad (1)$$

where $s = (n - 1)g^2\lambda/2$ and λ is the electron wavelength. (NB for the two-beam case $s = 0$ and $\xi_g^{eff} = \xi_g$.) Under weak beam conditions n and s are large and ξ_g^{eff} is essentially independent of the experimentally determined parameter ξ_g (Equation 1). For the 1 1 1, 2 0 0 and 2 2 0 reflections in PE16, errors in ξ_g become increasingly unimportant as n exceeds 5, 4 and 3, respectively. Large reductions in ξ_g are easily attainable leading to increased sensitivity in foil thickness measurements (Fig. 1).

3.3. Particle size measurement

Unbuckled areas, in which extinction contours run parallel to the foil edge, were selected. Micrographs were taken and their magnifications determined by calibrating the microscope after each investigation (Section 2.1). They were enlarged photographically to give average particle image sizes of at least 5 mm. The photographic enlargement was determined by measuring equivalent distances on the negatives and photographs.

A rectangular box aligned parallel to the extinction contours was drawn onto the photograph. It delineated a truncated wedge section of foil. Typically the box contained at least 100 clearly resolved particles. Its maximum thickness coincided with the onset of particle image overlap. All clearly resolved particles in the box were measured across their largest diameter using a Hewlett Packard 9874A digitizer interfaced to a programmable Hewlett Packard 9825A desk top calculator. A program was written to sort individual particle sizes into a size distribution of typically 8 to 10 equal size intervals. The number of particles per interval was scaled up to the total number of particles in the box and the overall mean particel size determined.

3.4. Volume fraction determination

Both the measured size distribution and foil thickness may need correction before determination of the volume fraction. Two extreme cases are considered:

(i) Particles and matrix electropolish at the same rate (Fig. 2a). Here particles centred outside the foil appear undersized: the measured size distribution is biased towards small particles. A correction of the "Crompton" type is applied [11].

(ii) Particles do not electropolish and remain

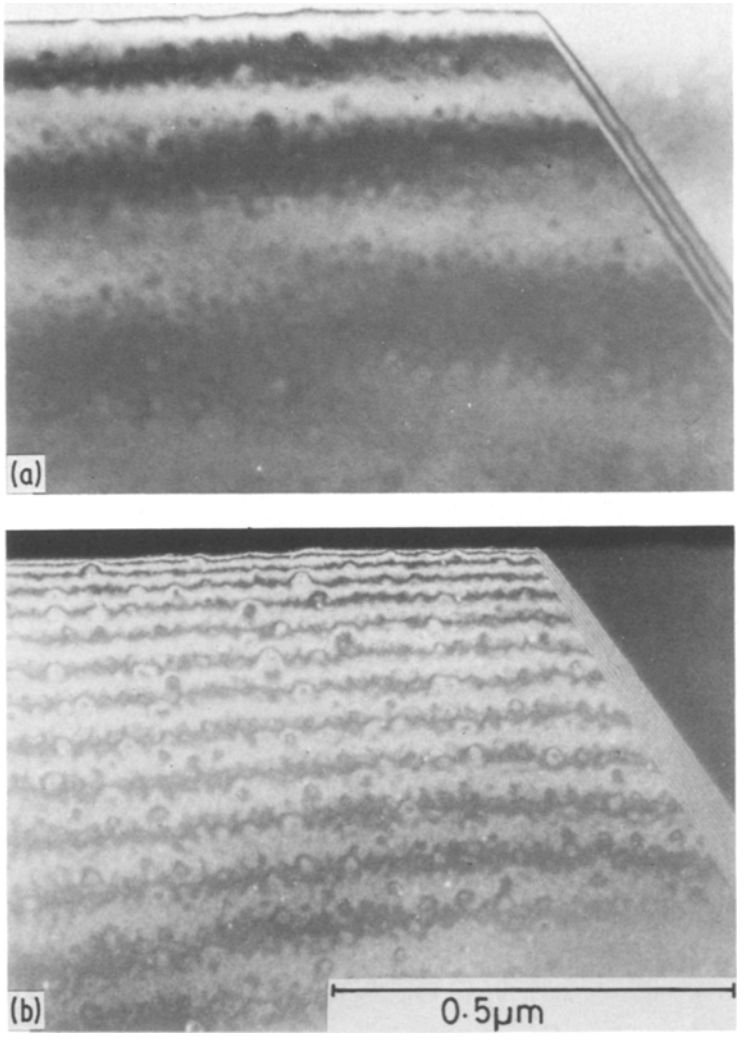

Figure 1 Foil thickness measurements using (a) standard 2-beam ($g = 1\,1\,1$, $n = 0$, $\xi_g = 28\,\text{nm}$) and (b) weak beam ($g = 1\,1\,1$, $n = 5$, $\xi_g^{\text{eff}} = 5.7\,\text{nm}$) conditions. The reduced extinction distance in (b) leads to increased sensitivity.

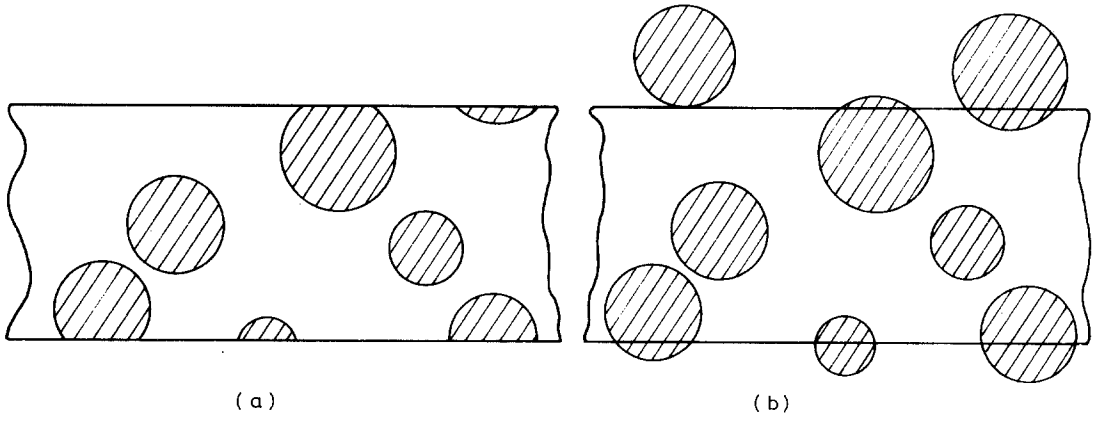

Figure 2 The observed particle size and volume fraction data may require correction because of differential electropolishing effects. The cases shown schematically in (a) and (b) are corrected using the "Crompton" and "$t_f + d$" procedures, respectively.

fixed to the foil until dissolution of the surrounding matrix (Fig. 2b). Here the measured foil thickness is effectively too thin for particles centred outside the foil. A correction of the "$t_f + d$" type is applied [12]: an effective thickness $(t_f + \bar{d}_i)$ is assigned to each size interval, t_f being the measured foil thickness, $\bar{d}_i$ the mean diameter of that interval.

The case where particles electropolish faster than the matrix is not considered: foils in which particles had polished away were rare and never used in volume fraction analyses.

A program was written to include both Crompton and $(t_f + d)$ correction procedures. The corrected size distributions were analysed with reference to the total number of particles in the box and the box volume. Three parameters were determined for each case; the corrected mean particle size $(\bar{d})$, the particle number density (ρ) and the volume fraction (f). The errors incurred are discussed in Section 5.1.

4. STEM results

4.1. SEM

Fig. 3 shows SEM micrographs of foils electropolished in (a) 10% perchloric acid/90% methanol cooled to -60° C, (b) 10% perchloric acid/90% 2-butoxyethanol at room temperature, and (c)

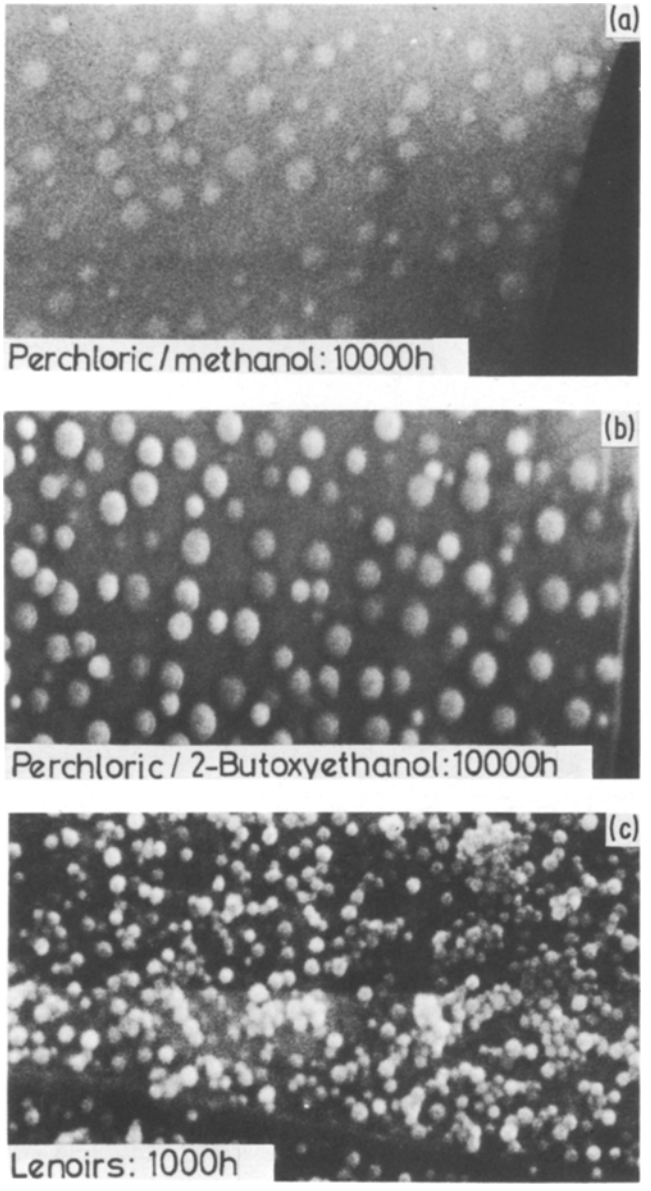

Figure 3 SEM images of foils electropolished in solutions of (a) perchloric acid/methanol, (b) perchloric acid/2-butoxyethanol and (c) Lenoirs solution. The flat contrast of (a) indicates that particles and matrix electropolish at approximately the same rate. The stronger contrast of (b) and (c) indicates that the particles remain unattacked during electropolishing.

Lenoirs solution at room temperature. Samples (a) and (b) were aged for 10 000 h. Sample (c) was aged for 1000 h.

The poor contrast of Fig. 3a indicates that the γ' particles and matrix electropolish at similar rates in perchloric/methanol foils. Thus true particle sizes and volume fractions are likely to be close to the Crompton corrected values. The relatively stronger contrast of Figs. 3b and c indicates that the particles remain essentially unattacked in perchloric/2-butoxyethanol and Lenoirs foils: they are assumed to stay in contact with the foil until dissolution of the surrounding matrix.

4.2. TEM: perchloric/methanol foils

Fig. 4 shows an age sequence of γ' particles in alloy I. The measured and corrected data are given in Table II.

Prolonged ageing results in increased average particle sizes and reduced particle number densities (Figs. 5a and b). The mean Crompton and $(t_f + d)$ values are used: similar results are obtained using each set individually. Linear regression

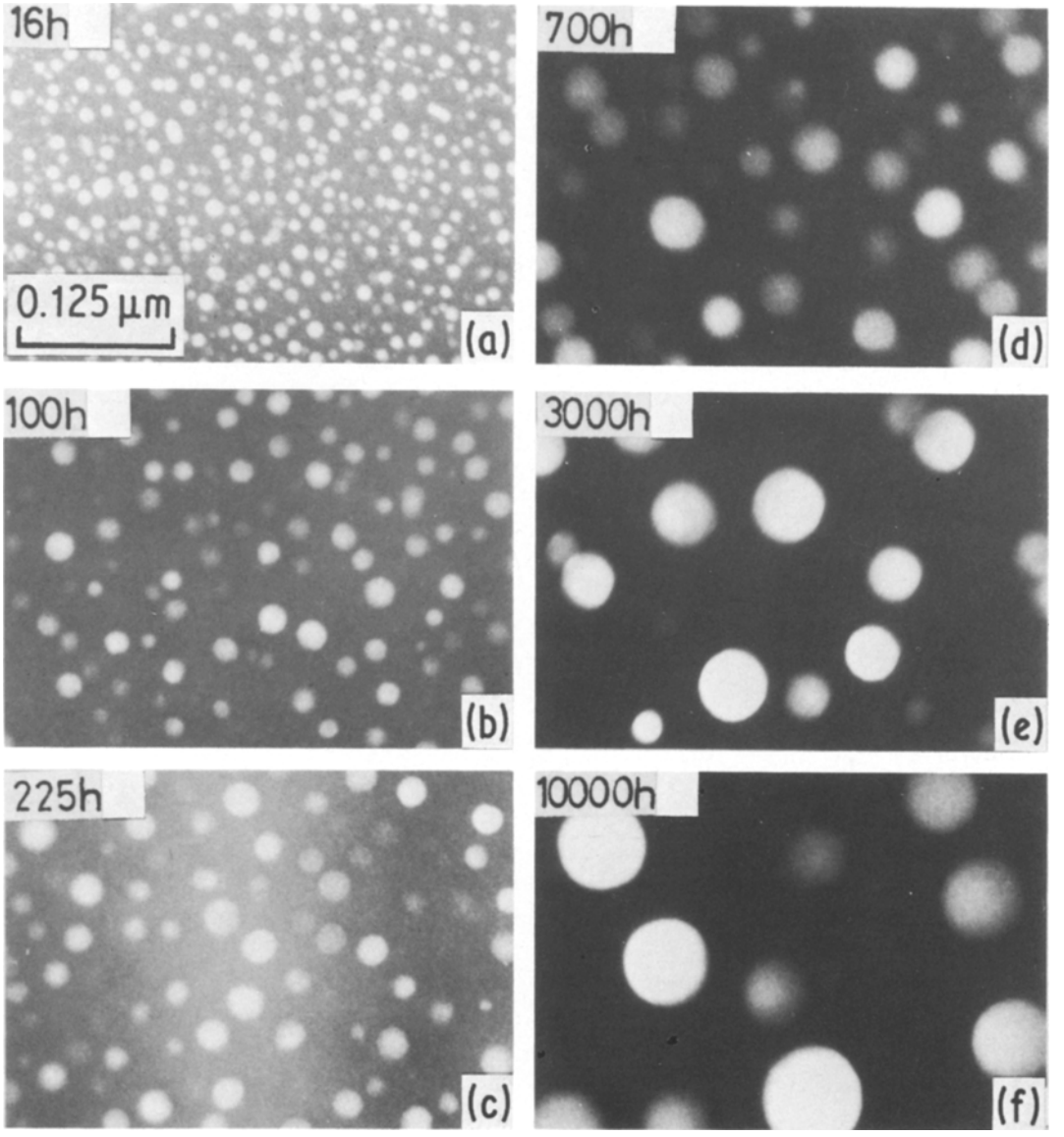

Figure 4 γ' particles in alloy I after (a) 16 h, (b) 100 h, (c) 225 h, (d) 700 h, (e) 3000 h and (f) 10 000 h ageing time at 700° C.

TABLE II Measured and corrected γ' particle parameters ($d \equiv$ particle diameter; $\rho \equiv$ particle number density; $f \equiv$ volume fraction)

	$\bar{d}_{observed}$ (nm)	$\bar{d}_{Cr}$ (nm)	$\bar{d}_{t_f+d}$ (nm)	ρ_{Cr} (m^{-3})	ρ_{t_f+d} (m^{-3})	f_{Cr} (%)	f_{t_f+d} (%)	$(f_{Cr} + f_{t_f+d})/2$ (%)
Alloy I								
16 h	9.5	9.9	9.3	2.0×10^{23}	2.0×10^{23}	10.7	9.5	10.1
100 h	17.3	18.2	16.8	2.7×10^{22}	2.9×10^{22}	9.3	8.3	8.8
225 h	22.4	23.0	21.9	1.2×10^{22}	1.2×10^{22}	8.8	7.7	8.3
700 h	31.4	33.0	30.4	5.0×10^{21}	5.2×10^{21}	10.2	8.9	9.6
3 000 h	39.5	42.2	37.4	2.1×10^{21}	2.3×10^{21}	9.8	8.4	9.1
10 000 h	61.6	64.6	58.8	5.8×10^{20}	6.1×10^{20}	9.4	8.1	8.8
Alloy II								
2.5 h	7.2	7.4	7.2	2.4×10^{23}	2.5×10^{23}	5.8	5.3	5.6

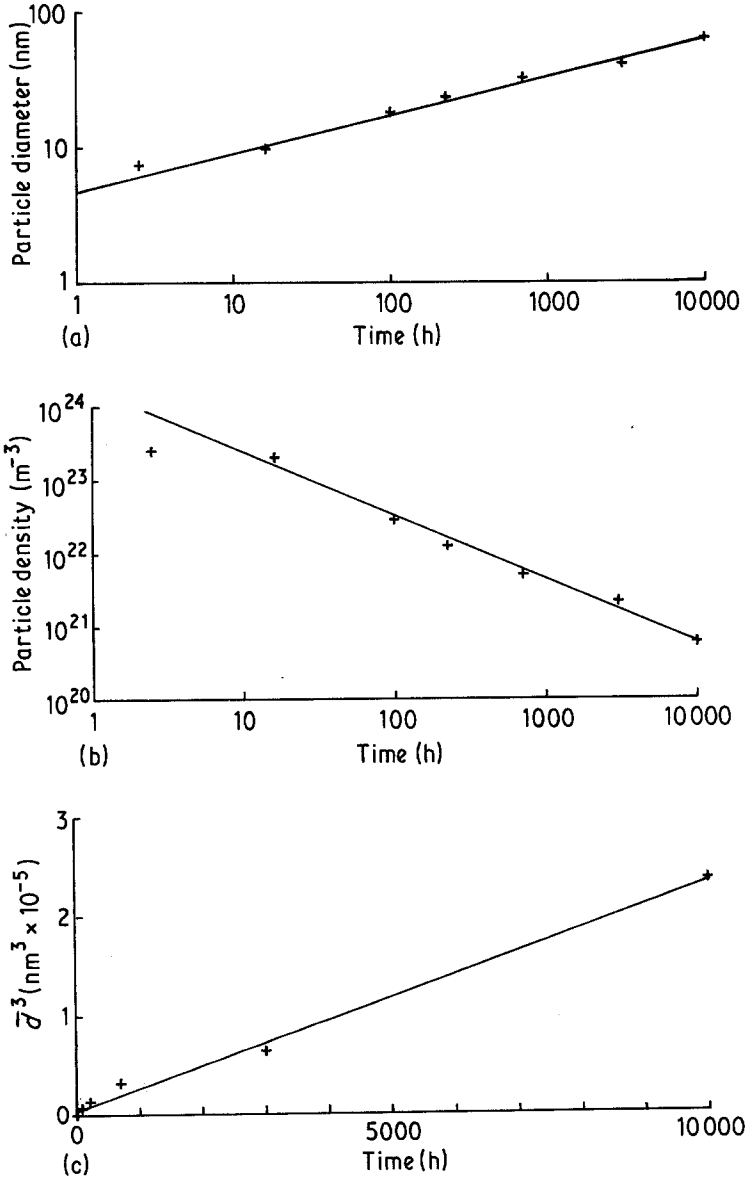

Figure 5 The variation of mean particle size ($\bar{d}$) and number density (ρ) with ageing for time (t). (a) log ($\bar{d}$) against log (t), (b) log (ρ) against log (t) and (c) $(\bar{d})^3$ against t.

analysis gives empirical fits as follows:

$$\bar{d} \propto t^{0.28}; \quad \rho \propto t^{-0.86}$$

where $\bar{d}$ is the average particle diameter, t is the ageing time and ρ is the particle number density. Swallow *et al.* [13] criticize the use of log/log plots. Their recommended $(\bar{d})^3$ against t plot is also given (Fig. 5c).

Errors of up to 24% may be incurred in volume fraction determinations (Section 5.1). The data for alloy I in Table II lie within 15% of the overall mean value of 9.1%. Thus the volume fraction appears to be invariant with ageing for times in excess of 16 h. For a given sample, the difference between corrected Crompton and $(t_f + d)$ values is typically 13%.

Fig. 6 shows non-spherical γ' particles coexisting with $M_{23}C_6$ particles after 10 000 h ageing at 700° C. The effect, most pronounced in dark field, is barely visible in bright field. It probably arises because of the long term reaction MC + $\gamma \rightarrow$ $M_{23}C_6 + \gamma'$, where MC and γ represent TiC particles and matrix, respectively [14]: the volume fraction of the spherical γ' particles is apparently unaffected (Table II).

A mean particle size of 7.3 nm is observed in alloy II aged for 2.5 h. The corresponding mean corrected volume fraction is only 5.6% (Table II).

4.3. TEM: perchloric/2-butoxyethonol foils

Foils electropolished in perchloric/2-butoxyethanol tend to be buckled. They are used in particle size measurements only.

Fig. 7 shows γ' particles in a sample aged for 10 000 h. Bright field images have a central "core" surrounded by a weak fringe (e.g. particles A in

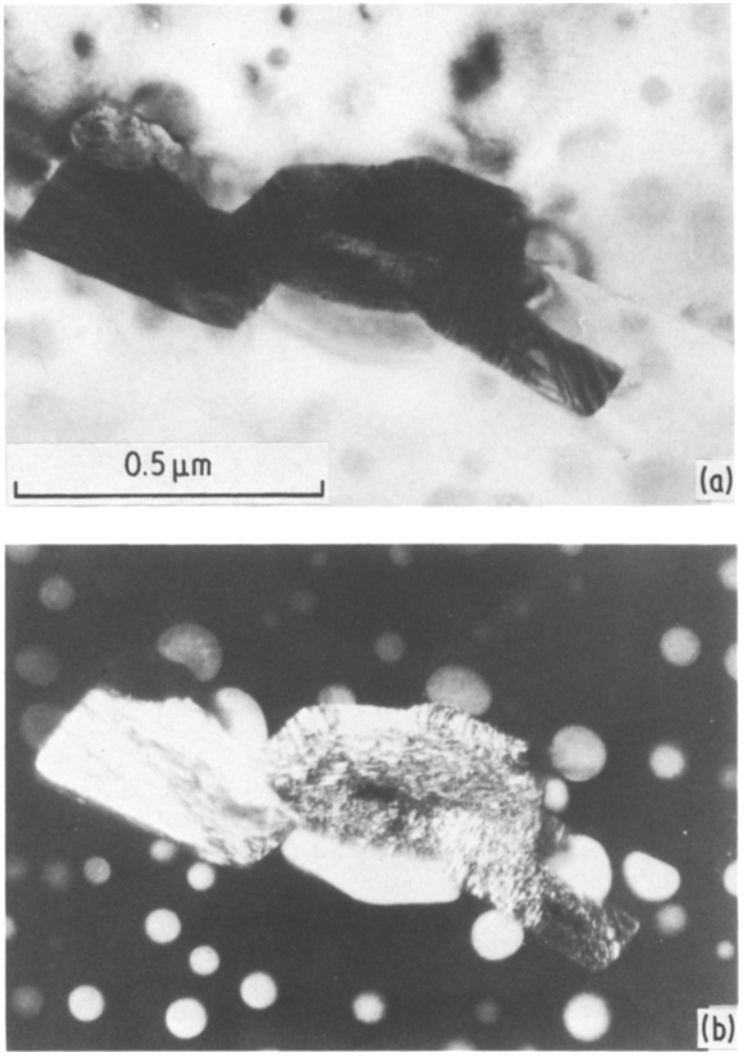

Figure 6 (a) bright and (b) dark field micrographs showing the co-existence of non-spherical γ' particles and $M_{23}C_6$ precipitates in alloy I after 10 000 h ageing at 700° C.

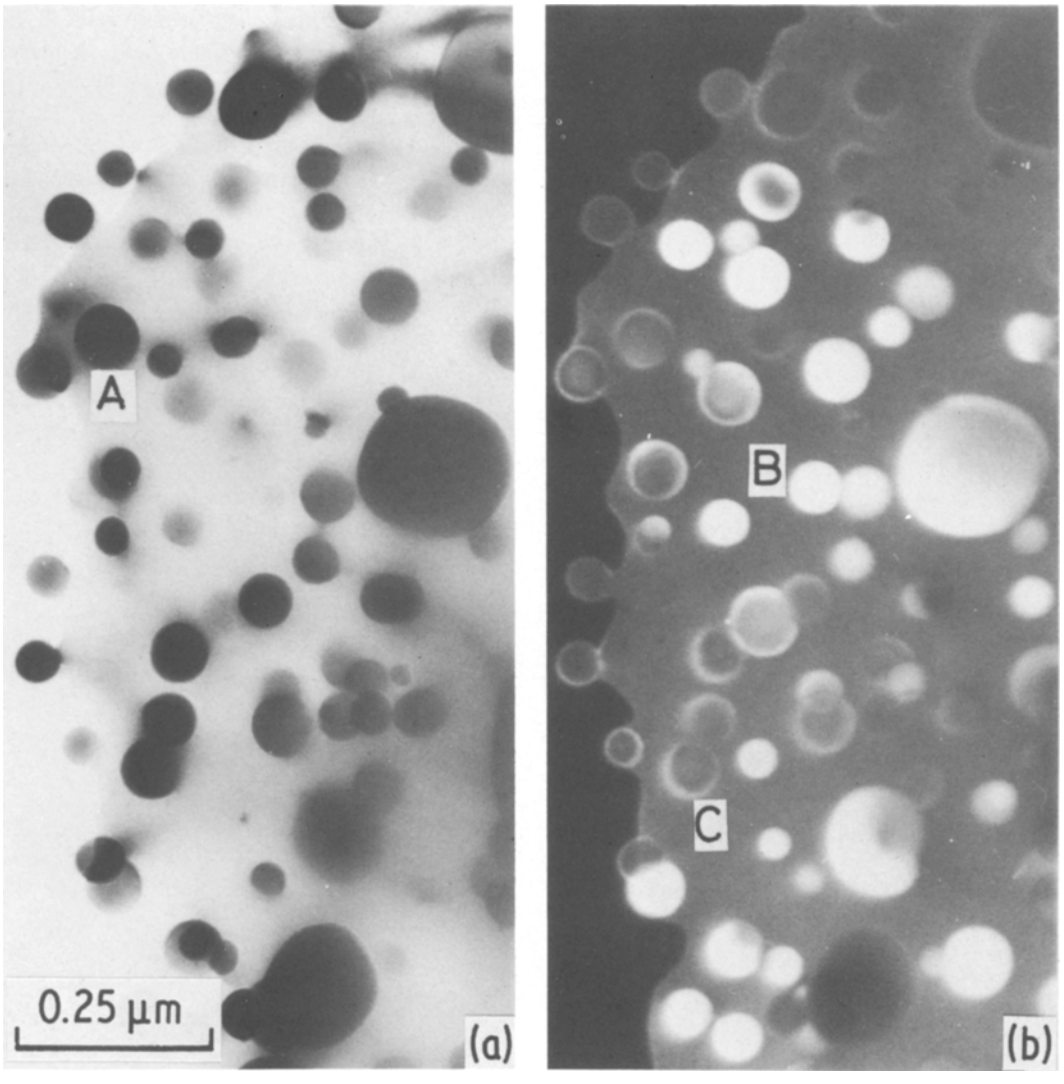

Figure 7 γ' particle images in perchloric/2-butoxyethanol foils. (a) bright field images have a central core surrounded by a fringe (particle A). (b) dark field images exhibit uniform contrast under 2-beam conditions (particle B) and ringed contrast elsewhere (particle C).

Fig. 7a). Dark field images exhibit uniform contrast under strongly diffracting 2-beam conditions and ringed contrast elsewhere (e.g. particles B and C, respectively, in Fig. 7b).

Because of foil buckling only a limited number of particles were measured in both bright and dark field micrographs. Comparable results were obtained by measuring the core region in bright field and the strongly diffracting region in dark field. The mean measured bright field diameter of 59.7 nm compares with a measured dark field diameter of 61.2 nm in perchloric/methanol foils.

4.4. TEM: Lenoirs foils

Fig. 8 shows γ' particles in a sample aged for 1000 h. The various particle images observed are shown schematically in Fig. 9. Bright field images generally have a central core, an intermediate shell and a weak outer fringe (e.g. particle A in Fig. 8a). Diameters d_1 across the shell and core, and d_2 across the core only, were measured. Dark field images appear as bright discs under 2-beam conditions: elsewhere they have a ring and core structure (particles B, C and D in Figs. 8b and c). Diameters d_3 of the 2-beam discs and d_4 and d_5 of the white and black cores were measured.

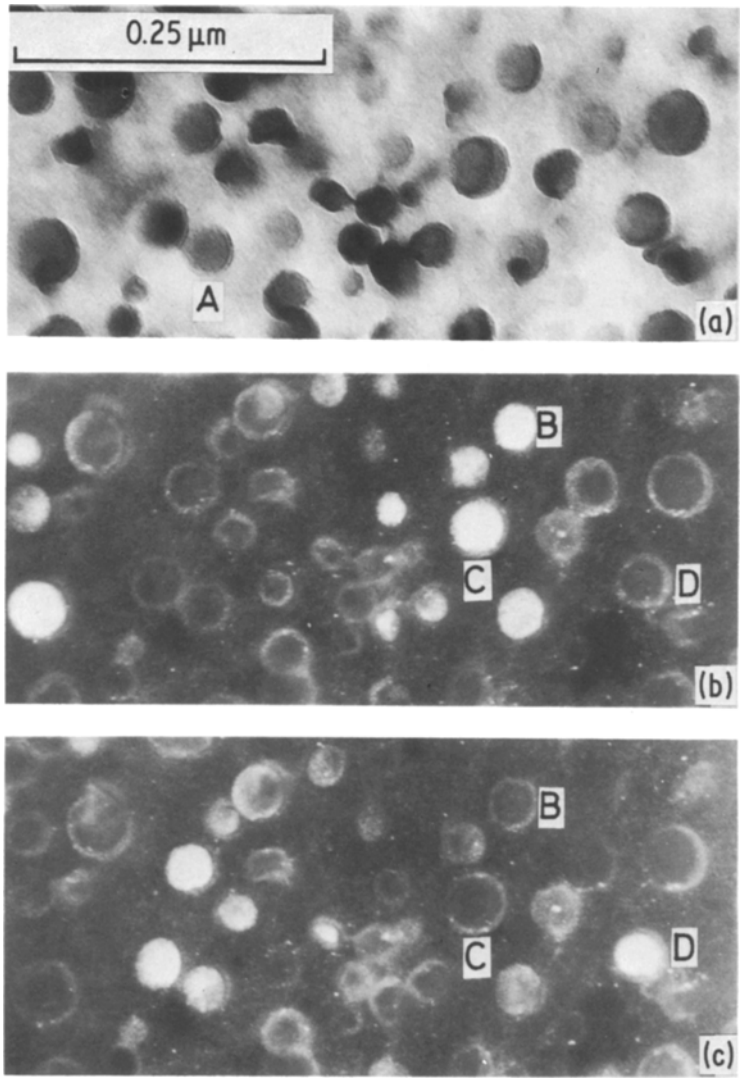

Figure 8 γ' particle images in Lenoirs foils. (a) bright field images have a central core, an intermediate shell and an outer fringe (particle A). (b) and (c) dark field images exhibit uniform contrast under 2-beam conditions and ringed contrast elsewhere (particles, B, C and D).

Table III shows the results obtained. A limited number of particles were imaged in both bright and 2-beam dark field conditions. In a population of 17 particles, the two bright field diameters differ by 16%. The small diameter agrees best with the dark field value. The same conclusion applies when the population is extended to 44 to include white and black core dark field images. In a more representative population of 107 particles, the bright field diameters d_1 and d_2 differ by 13%. Overall the data indicate that the bright field diameter ratio $(d_1 - d_2)/d_2 \sim 0.15$, and, that the three dark field diameters d_3, d_4 and d_5 are equivalent and equal to the smaller bright field diameter d_2.

5. Discussion

5.1. Errors incurred during particle size and volume fraction determination

Errors incurred, their sources and effects, are listed in Table IV. The largest errors arise through electropolishing effects ($\sim$ 10%), particle invisibility ($\sim$ 10%) and to a lesser extent incorrect values of the effective extinction distance ($\sim$ 4%). Maximum errors in the determined particle sizes and volume fractions are expected to be $\sim$ 10% and $\sim$ 24%, respectively.

5.2. Electropolishing effects

Different particle images were observed in the foils examined. They ranged from simple, well-defined,

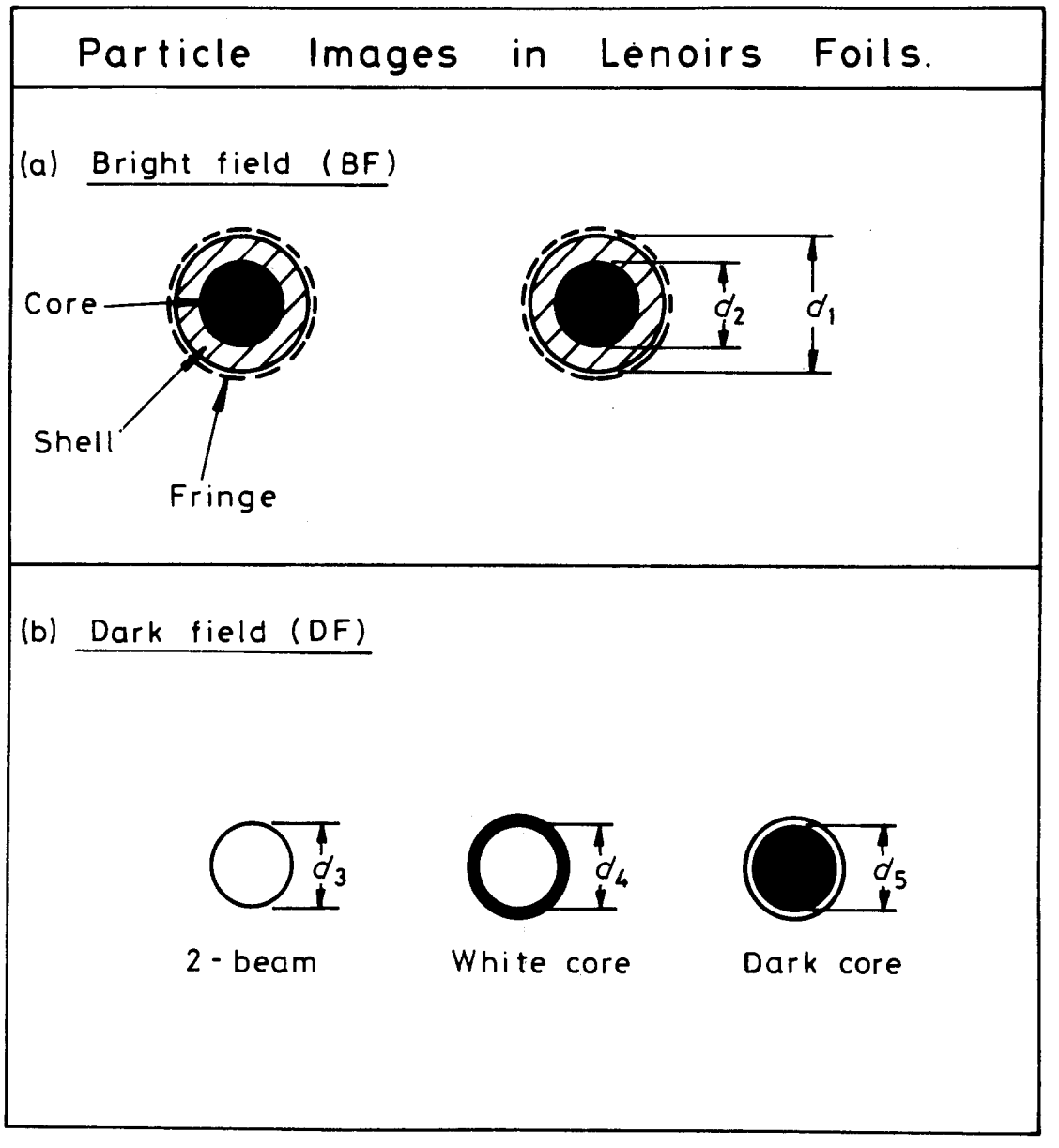

Figure 9 Schematic representation of the particle images observed in Lenoirs foils.

images in dark field micrographs of perchloric/methanol foils to complex, "core and shell", images in Lenoirs foils (Figs. 4 and 8, respectively). The corresponding image diameters differ by up to 15% (Sections 4.2 and 4.4). Dark field data from perchloric/methanol foils were used in the mean particle size and volume fraction determinations of Section 4.2. Similar data were obtained from the perchloric/2-butoxyethanol and Leniors foils by measuring only the core regions of bright and dark field images.

The SEM micrographs of Fig. 3 suggest that particles and matrix electropolish at similar rates in perchloric/methanol foils. They electropolish less quickly or not at all in the other foils. The complex TEM images seen in perchloric/2-butoxyethanol and Lenoirs foils may thus indicate the presence of differential electropolishing effects.

5.3. γ' particle size

Fig. 10 shows the γ' particle size data of Fig. 5a together with other data for PE16 aged at 700° C [1–3]. Empirical fits of the type $\bar{d} \propto t^n$ may be ascribed to each data set, $\bar{d}$ being the mean particle

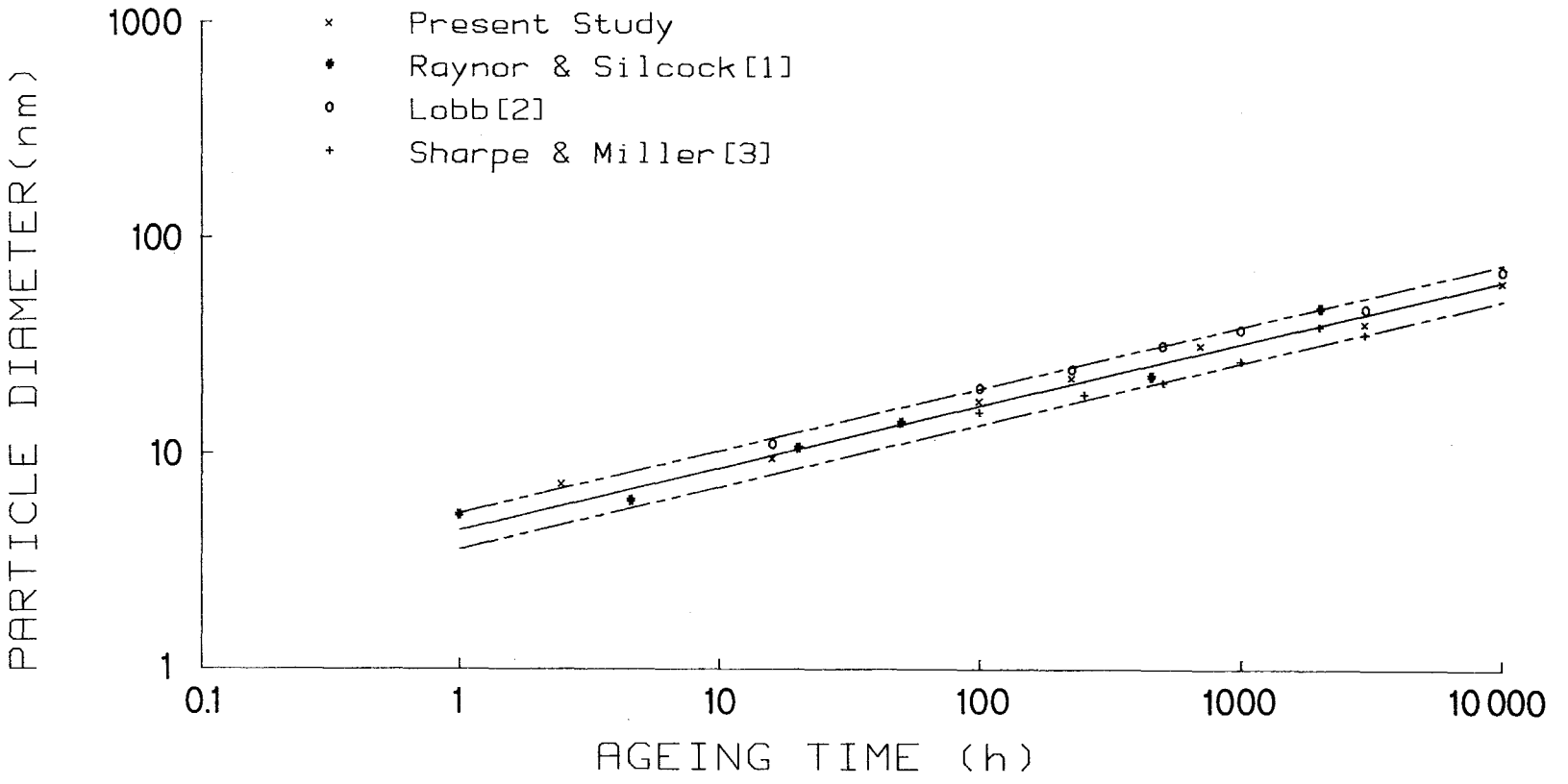

Figure 10 The variation in mean particle size with ageing in this and other investigations: best fit and scatter bands are shown by continuous and broken lines, respectively.

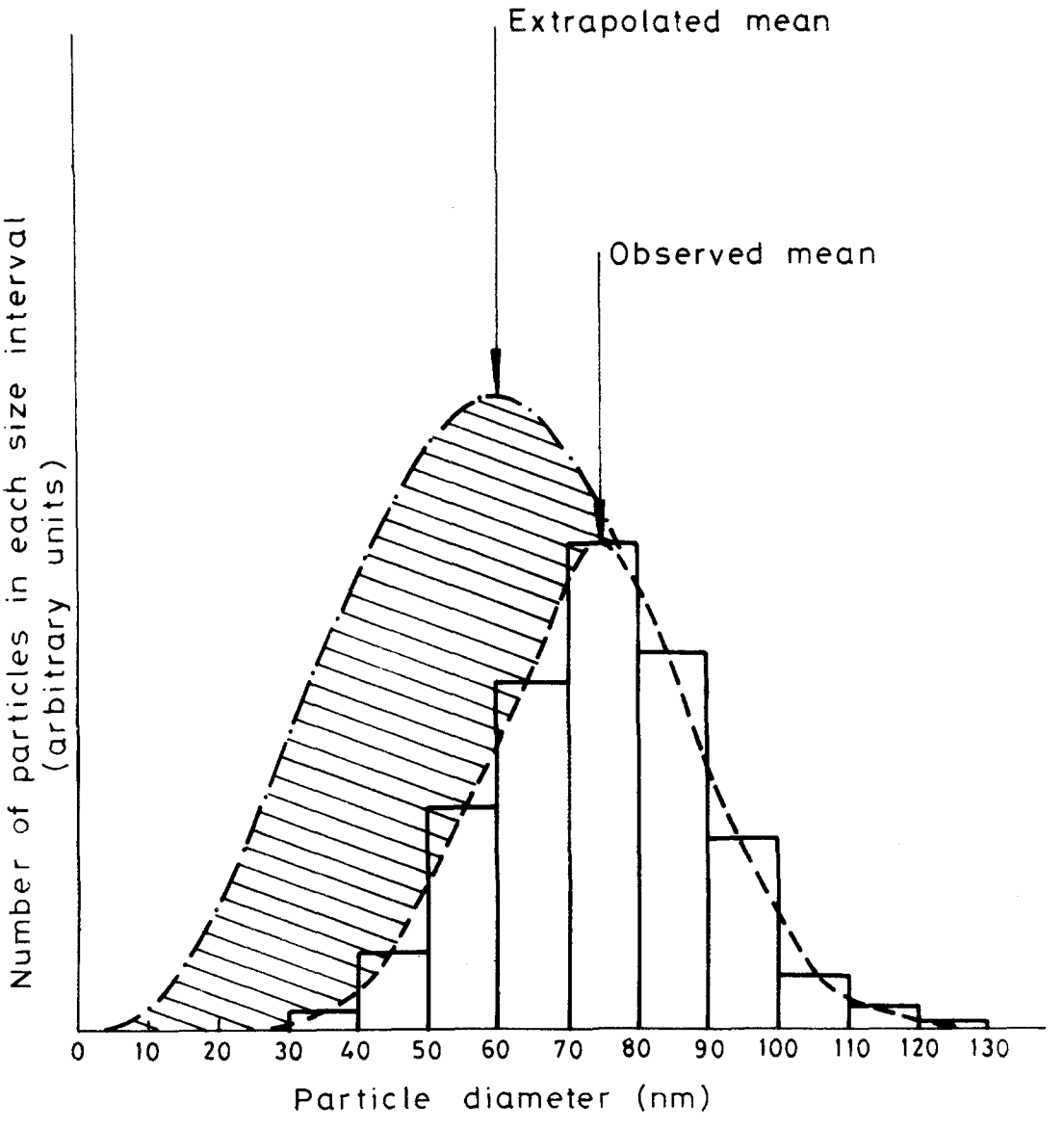

Figure 11 An investigation of possible particle invisibility effects in foils of alloy II aged for 2.5 h at 700° C. The observed size histogram is modelled to have a mean equal to that extrapolated from long age data. "Invisible" particles lie in the cross-hatched regions.

slight differences in their chemical composition both alloys lie within the specification of PE16 (Table I). Thus the complete γ' volume fraction appears to come out of solution between 2.5 and 16 h ageing at 700° C.

The observed maximum γ' volume fraction in alloy I is 9.1% (Section 4.2). This agrees with Raynor and Silcock's [1] value. A value of 14.7% is determined from the chemical composition of the alloy by assuming that all available titanium and aluminium precipitate out as γ' ($Ni_3(Ti, Al)$) except titanium already removed as TiC. Now Smith [15] observes no γ' precipitation in a special cast of PE16 containing only 0.38 wt % Ti, 0.35 wt % Al and 0.045 wt % C. Taking his figures to represent the solid solubility limits of titanium and aluminium in the presence of TiC precipitation, an upper limit of 10.8% is estimated for the maximum γ' volume fraction precipitated in alloy I. This figure is in good agreement with observation. The particle sizes used in the volume fraction determinations of Section 4.2 could have been 10 to 15% larger if measured in bright field micrographs of Lenoirs foils (Section 4.4). The

corresponding maximum volume fractions of 12.4 and 14.1%, respectively, are higher than the estimated value. Thus the particle sizes used, those measured in dark field micrographs of perchloric/methanol foils, are most likely correct.

5.5. Particle number density

A relationship may be derived for the particle number density/age time dependence in samples aged at 700° C for between 16 and 10 000 h, by making the following assumptions:

(i) the complete volume fraction f is out of solution;

(ii) the particle sizes may be represented by the mean particle size. Thus,

$$f = \frac{\pi}{6}(\bar{d}_1)^3\rho_1 = \frac{\pi}{6}(\bar{d}_2)^3\rho_2 \qquad (2)$$

where $\bar{d}_i$ and ρ_i are mean particle diameter and particle number density, respectively, measured after ageing for a time t_i. Now

$$\bar{d}_i \propto t_i^n,$$

thus

$$\rho_i \propto t_i^{-3n}.$$

Since $n = 0.28$ for alloy I (Section 4.2), $\rho \propto t^{-0.84}$. This is in good agreement with the empirical fit for the particle number density data in Fig. 5.

Kirkwood [16] has studied γ' particles in a nickel-based alloy aged for up to 16 h at 750 and 800° C. His data approach a $\rho \propto t^{-1.0}$ dependence, with the time exponent less negative than -1.0. Kirkwood's data is thus consistent with that of Fig. 5.

6. Conclusions

1. A TEM technique has been developed which enables γ' particle sizes and volume fractions to be determined quickly and reliably. For PE16, the corresponding maximum errors are estimated to be ~10% and ~24%, respectively. Data collected from thin foil samples electropolished to perforation in three different solutions were compared. Foils electropolished in 10% perchloric acid/90% methanol solution cooled to −60° C proved to be the most suitable.

2. The results obtained indicate that complete γ' precipitation occurs between 2.5 and 16 h ageing at 700° C. Thereafter up to 10 000 h the mean particle size ($\bar{d}$) and the particle number density (ρ) vary with age time (t) in accordance with the following empirical relationships:

$$\bar{d} \propto t^{0.28}; \quad \rho \propto t^{-0.86}.$$

3. The maximum γ' volume fraction was found to be 9.1% in agreement with a best estimate value of 10.8% based on chemical composition arguments.

Acknowledgement

This paper is published by permission of the Central Electricity Generating Board.

References

1. D. RAYNOR and J. M. SILCOCK, "Strengthening Mechanisms in γ' Precipitating Alloys", CEGB Report No. RD/L/R1613 (1969).
2. R. C. LOBB, unpublished work (1978).
3. R. M. SHARPE and W. N. MILLER, unpublished work, Dounreay Nuclear Establishment (1974).
4. V. MARTENS and E. NEMBACH, *Acta Metall.* **23** (1975) 149.
5. D. S. GELLES, in Proceedings of the Tenth International Symposium on Effects of Radiation on Materials, Savannah, Georgia, June 1980, edited by D. Kramer, H. R. Brager and J. S. Perrin ASTM STP 725 (American Society for Testing and Materials, Philadelphia, 1981) p. 562.
6. C. G. WINDSOR and V. S. RAINEY, "Small Angle Neutron Scattering (SANS) from Heat Treated PE16 Specimens from Berkeley Nuclear Laboratories" AERE (Harwell) Report No. R10523 (1982).
7. C. G. WINDSOR, V. S. RAINEY, P. K. MADDEN and V. M. CALLEN, to be published (1983).
8. P. B. HIRSCH, A. HOWIE, R. B. NICHOLSON, D. W. PASHLEY and M. J. W. WHELAN, "Electron Microscopy of Thin Crystals" (Butterworths, London, 1965) p. 202.
9. C. F. BILSBY, PhD thesis, Cambridge (1966).
10. D. J. H. COCKAYNE, I. L. F. RAY and M. J. WHELAN, *Phil. Mag.* **20** (1969) 1265.
11. J. M. G. CROMPTON, R. M. WAGHORNE and G. B. BROOK, *Brit. J. Appl. Phys.* **17** (1966) 1301.
12. C. M. SELLARS and A. F. SMITH, *J. Mater. Sci.* **2** (1967) 521.
13. G. A. SWALLOW, R. J. WHITE and S. B. FISHER, "Anomalous Particle Coarsening in Nimonic PE16" CEGB Report No. RD/B/N2966 (1974).
14. R. F. DECKER and C. T. SIMS, "The Superalloys", edited by C. T. Sims and W. C. Hagel (John Wiley and Sons Inc., New York, 1972) P. 33.
15. K. B. SMITH, unpublished work (1973).
16. D. H. KIRKWOOD, *Acta Metall.* **18** (1970) 563.
17. J. W. EDINGTON, "Practical Electron Microscopy in Materials Science" (MacMillan Press Ltd, London and Basingstoke, 1975) Monograph 3.

Received 11 March
and accepted 18 March 1983